Available online at www.sciencedirect.com
ScienceDirect
Journal of Catalysis 249 (2007) 250–260
JOURNAL OF CATALYSIS
www.elsevier.com/locate/jcat

# Propane dry reforming to synthesis gas over Ni-based catalysts: Influence of support and operating parameters on catalyst activity and stability

L.B. Råberg [a], M.B. Jensen [a], U. Olsbye [a,*], C. Daniel [b], S. Haag [b], C. Mirodatos [b], A. Olafsen Sjåstad [a,c]

[a] *Department of Chemistry, Center for Materials Science and Nanotechnology, University of Oslo, P.O. Box 1033 Blindern, N-0315 Oslo, Norway*
[b] *Institut de Recherches sur la Catalyse, CNRS, 2 Avenue A. Einstein, 69626 Villeurbanne, France*
[c] *SINTEF Materials and Chemistry, P.O. Box 124 Blindern, N-0314 Oslo, Norway* [1]

Received 23 January 2007; revised 28 March 2007; accepted 3 April 2007

Available online 11 June 2007

**Abstract**

A series of supported Ni catalysts (∼2 wt% Ni) were tested for the dry reforming of propane to synthesis gas reaction at 600 °C, $C_3H_8$:$CO_2$:$H_2$:$N_2$ (%) = 10:30:10:50, 1 atm and GHSV = 13333 Nml/(h $g_{cat}$). The support systems studied range from acidic ($SiO_2$) to amphoteric [$Al_2O_3$, Mg(Al)O] to basic oxides [MgO, CaO], with BET areas of 100, 100 (131 and 173), 117, and 16 $m^2$/g, respectively. Ni particle size and reduction state was investigated by magnetic measurements, performed before and during catalytic testing. Support basicity was measured by $CO_2$ TPD. It was observed that the intrinsic activity of the catalysts (TOF) depends strongly on the Ni particle size ($D$) in the size range of 4.5–11 nm. As such, a TOF versus $D$ plot showed an exponential inverse relationship, much more pronounced than previously reported for the methane dry reforming reaction. In turn, a volcano-type correlation was found between intrinsic catalyst activity and support basicity. As a result, the best catalytic performance, including a low selectivity to methane, was observed on the most dispersed Ni particles supported on Mg(Al)O. Key mechanistic features were derived from these observations.


*Keywords:* Propane dry reforming; Methane dry reforming; Synthesis gas; Ni catalysts; Ni particle size; Support basicity

## 1. Introduction

Synthesis gas (CO and $H_2$) production represents a step of major importance in the conversion of natural gas to fuels and petrochemical products. Currently, the main process for converting natural gas to synthesis gas is reforming with steam or carbon dioxide. Supported Ni catalysts are the preferred choice as catalysts for the reforming reaction, due to the low cost and easy availability of Ni metal. The main disadvantage of Ni/support catalysts compared with noble metal catalysts is a lower stability with respect to carbon deposition (see [1] and Refs. therein). Many attempts have been made to improve the stability of Ni-based reforming catalysts, with using a basic support among the most successful approaches [1–6]. Whether the improved effect is due to oxygen transfer from the basic oxide to the metal [7–10], to electronic effects [11] or to a higher dispersion of the metal [12] remains a matter of debate.

Although numerous articles exist on the catalytic dry reforming of methane to synthesis gas [13], only few studies have addressed the specificity of propane dry reforming using supported metal catalysts (e.g., Rh, Ru, Re) [14–16]. Recently, we extended our previous studies of methane dry reforming over Ni-based catalysts toward propane dry reforming [10,17] occurring through the following reaction:

$$C_3H_8 + 3CO_2 \rightarrow 6CO + 4H_2. \quad (1)$$

This choice was based on the lower vapor pressure of propane compared with methane at ambient temperature, making it more suitable for use in, say, fuel cell cars with internal reforming.

* Corresponding author. Fax: +47 22855441.
*E-mail address:* unni.olsbye@kjemi.uio.no (U. Olsbye).
[1] Present address: a.

0021-9517/$ – see front matter 
doi:10.1016/j.jcat.2007.04.004

In the present work, we address the possible correlation between support basicity and Ni/support activity and stability of catalysts for the dry reforming of propane to synthesis gas by a multitechnique approach. The activity, selectivity, and stability of supported Ni catalysts were investigated by catalytic testing in a conventional fixed-bed reactor. The support systems studied range from weakly acidic ($SiO_2$) to amphoteric [$Al_2O_3$, Mg(Al)O] to basic oxides [MgO, CaO]. The Ni particle size and reduction state was investigated by magnetic measurements performed before and during catalytic testing. Temperature-programmed desorption (TPD) using $CO_2$ as probe molecule was used to rank the supports with respect to basicity. Turnover frequencies (TOFs) for each catalyst were calculated on the basis of metal dispersion as a guideline for addressing the relative importance of support acid–base properties and metal distribution, respectively.

## 2. Experimental

### 2.1. Catalyst preparation and characterization

$Ni/SiO_2$ was synthesized by calcining $SiO_2$-40 (Fluka, grain size 0.2–0.3 mm) at 825 °C for 10 h before impregnating it with an aqueous solution of nickel nitrate. After impregnation, the product was dried overnight at 100 °C and calcined at 750 °C for 8 h in air.

$Ni/Al_2O_3$ was prepared by impregnating $\delta$-$Al_2O_3$ Puralox SCCa-90 (Condea) with an aqueous solution of nickel nitrate before drying it in air at 100 °C. The material thus obtained was then calcined for 8 h at 750 °C in air.

Ni/MgO and Ni/CaO were prepared by synthesizing the corresponding hydroxides, $Mg_{0.98}Ni_{0.02}(OH)_2$ and $Ca_{0.98}Ni_{0.02}(OH)_2$, by coprecipitation at constant pH ($12.0 \pm 0.1$) at $40 \pm 2$ °C in a specially designed apparatus. During synthesis, the two reactant solutions A ($OH^-$ balanced by $K^+$; ≈250 ml) and B ($Mg^{2+} + Ni^{2+}$ or $Ca^{2+} + Ni^{2+}$ balanced by $NO_3^-$; 80 ml), as well as the product solution C (initially 160 ml of degassed deionized water), were kept at constant temperature in a water bath. The whole system was kept under inert conditions by Ar flushing. The pH was controlled through a feedback loop using a pH meter, which activated or stopped the pump for source solution A. Source solution B was added at a constant rate into the product solution C via a second pump. The mixing of reactant solutions (A and B) to yield the product solution (C) was completed within approximately 1 h, followed by stirring for approximately 1 h for the $Mg_{0.98}Ni_{0.02}(OH)_2$ and 19 h for the $Ca_{0.98}Ni_{0.02}(OH)_2$. The products thus obtained were washed in a diluted $NH_4OH$ solution and dried overnight at 90 °C. Phase purity of the samples was confirmed by powder X-ray diffraction (XRD). No reflections from $KNO_3$ or carbonate phases of Mg or Ca were observed. The hydroxides were converted into the corresponding oxides in a fluidized-bed reactor maintained at 650 °C (Mg–Ni–O) and 750 °C (Ca–Ni–O) in $N_2$ atm for 14 h. The samples were then cooled to room temperature under inert conditions.

The Ni/Mg(Al)O catalysts (types I and II) were prepared by first synthesizing the corresponding hydrotalcite-like material with nominal composition $Mg_{5.88}Ni_{0.12}Al_2(OH)_{16}CO_3 \cdot nH_2O$ and $(Mg + Ni)/Al = 3$ by coprecipitation at constant pH ($11.5 \pm 0.1$) and temperature ($40 \pm 2$ °C) in the same apparatus described earlier. During synthesis, the two reactant solutions A ($CO_3^{2-}$ and $OH^-$ balanced with $K^+$; ≈730 ml) and B ($Mg^{2+} + Ni^{2+} + Al^{3+}$ balanced with $NO_3^-$; 250 ml), as well as the product solution (initially containing 500 ml of deionized water), were kept at constant temperature in a water bath. The pH was controlled through a feedback loop using a pH meter, which activated or stopped the pump for the source solution A. Source solution B was added at a constant rate into the product solution via a second pump. The mixing of reactant solutions to yield the product solution was completed within approximately 3 h, followed by stirring for approximately 1 h. The product thus obtained was washed and dried overnight at 90 °C. Powder XRD showed that this hydrotalcite-like material was a pure phase (i.e., no reflections from the potential contaminant $KNO_3$ or from other phases were observed). The hydrotalcite-like material, $Mg_{5.88}Ni_{0.12}Al_2(OH)_{16}CO_3 \cdot nH_2O$, was subjected to one of several calcination programs, resulting in catalysts designated types I and II. The type I Ni/Mg(Al)O catalyst was obtained by first calcining the corresponding hydrotalcite-like phase in two steps at 400 and 800 °C under vacuum before activating it by Zr reduction using chips of Zr in evacuated sealed silica glass ampules. Zr was positioned in a crucible inside the ampule to separate it from the catalytic material. Both Zr and Ni/Mg(Al)O were held at 600 °C for 7 days before cooling to room temperature. Small amounts of oxygen were finally leached into the ampule to passivate the nickel particles. Ni/Mg(Al)O (type II) was prepared by performing the calcination and activation steps simultaneously by sending a flow of 10% $H_2$ in $N_2$ at 650 °C over the hydrotalcite-like material for 14 h in a fluidized-bed reactor before cooling it to ambient temperature under the same atmosphere. Then the material was passivated at room temperature in a 2% $O_2$ in $N_2$ flow for 1 h. The main difference in the activation procedures for types I and II is that type I was activated under water-free conditions, whereas type II was activated in the presence of humidity (because calcination and activation occur simultaneously).

Nickel loading (ICP-AES) and specific surface areas (1-point BET) of the Ni/support systems (reduced and passivated, see below) are listed in Table 1.

Table 1
Ni loading and specific surface area of passivated Ni/support systems

| | Ni loading (wt%) | Specific surface area ($m^2/g$) |
|---|---|---|
| $Ni/SiO_2$ | 1.9 | 100 |
| $Ni/Al_2O_3$ | 1.8 | 100 |
| Ni/Mg(Al)O I | 1.6 | 131 |
| Ni/Mg(Al)O II-c | 1.8 | 173 |
| Ni/MgO-b | 1.8 | 117 |
| Ni/CaO | 2.8 | 16 |

### 2.2. Catalytic testing

The catalysts (0.45 g sieved to grain size of 0.18–0.30 mm) were tested in a tubular quartz fixed-bed reactor with an inner diameter of 6 mm. The temperature in the catalyst bed was measured by a thermocouple placed in a quartz well (3 mm o.d.) inside the reactor. $Ni/SiO_2$, $Ni/Al_2O_3$, and Ni/MgO a and b were activated in situ in a flow of 100 Nml/min 10% $H_2$ in $N_2$ for 14 h at 650 °C before the system was cooled to the test temperature of 600 °C, whereas Ni/CaO was heated in a flow of $H_2$:$CO_2$:Ar (%) = 10:30:60. When Ni/CaO was heated under a $H_2$ in $N_2$ flow, a rapid temperature increase was observed when switching to the feed gas mixture at 600 °C, probably due to (partial) conversion of the CaO support to $CaCO_3$. To avoid sintering of the Ni particles due to overheating at the onset of the reactant feed, Ni/CaO was gradually converted to the carbonate phase during heating/reduction. No overheating occurred when this catalyst was heated in a $H_2/CO_2$ mixture or when the other catalysts were heated in $H_2$ in $N_2$. Ni/Mg(Al)O (types I and II) were heated directly to 600 °C in 10% $H_2$ in $N_2$. On reaching the test temperature, the feed gas composition was changed to reforming conditions [$C_3H_8$:$CO_2$:$H_2$:$N_2$ (%) = 10:30:10:50] with a total flow rate of 100 Nml/min [GHSV = 13,333 Nml/(h $g_{cat}$)]. $H_2$ was added to the feed to keep the catalysts in a reduced state even at moderate conversion, because it had previously been observed that a 1.9 wt% Ni/Mg(Al)O catalyst was oxidized with time on stream under a $C_3H_8$:$CO_2$:$N_2$ (%) = 20:60:20 flow at 600 °C and moderate (<40%) conversion [10]. Water produced during the reaction was collected in a water trap, and the dry effluent was analyzed by a 3 columns Agilent micro gas chromatograph. The effluent was found to contain significant amounts of $CO_2$, $C_3H_8$, $H_2$, $N_2$, CO, and $CH_4$. In addition, $C_2H_4$ was always observed, but at concentrations <1%.

Methane dry reforming was tested over Ni/Mg(Al)O II with $CH_4$:$CO_2$:$H_2$:$N_2$ (%) = 10:30:10:50, with all other parameters being equal to those in the propane-reforming test.

### 2.3. Magnetic measurements

Magnetic measurements were performed at ambient temperature by the Weiss extraction method [18] in an electromagnet providing fields up to 21 kOe. Information on the degree of Ni reduction and on the mean diameter of the Ni metal particles ($D$) was extracted from the magnetization isotherm [19]. The degree of Ni reduction was calculated from the saturation magnetization ($M_s$). For ferromagnetic materials, a residual magnetic moment remains at zero field after exposure to a magnetic field; however, when the particle diameter drops below a certain size ($D_c$), the ferromagnetic particles become superparamagnetic [19]. Absence of remanent magnetization ($M_r$) indicates superparamagnetic behavior [19]. Under such conditions, the mean sizes of large ($D_1$) and small ($D_2$) Ni particles can be calculated according to Langevin's equation [19]. The accuracy of the method is assumed to be within ±20% [18]. The mean particle diameter was calculated as $D = (D_1 + D_2)/2$. In the applied magnetic setup, it was empirically determined that $D_c$ for Ni was 15 nm and that the ratio $2M_r/M_s$ gave the fraction of particles with larger size than the critical diameter.

Before the magnetic measurements, $Ni/SiO_2$, $Ni/Al_2O_3$, Ni/MgO, and Ni/CaO were activated in a separate reactor at 650 °C for 14 h in a flow of 10% $H_2$ in $N_2$ before the reactor was cooled to room temperature and the surface of the generated nickel particles was passivated by a gas flow of 2% $O_2$ in $N_2$ for 1 h.

Then ∼200 mg of $Ni/SiO_2$, $Ni/Al_2O_3$, Ni/Mg(Al)O (types I and II-c), Ni/MgO-b, and Ni/CaO were loaded into a specially designed fixed-bed reactor that was adapted for both magnetic measurements and catalytic testing [20]. All of the materials except Ni/CaO were first reduced in situ by heating to 600 °C (10 °C/min) in a flow of 45 Nml/min of 10% $H_2$ in $N_2$ (with Ni/CaO reduced in 10% $H_2$ and 30% $CO_2$ in $N_2$) before switching to $N_2$, isolating the reactor, quenching it to room temperature, and loading it into the electromagnet to collect the magnetization isotherm. Thereafter the reactor was exposed to reforming conditions [600 °C, 45 Nml/min of $C_3H_8$:$CO_2$:$H_2$:$N_2$ (%) = 10:30:10:50 (GHSV = 13500 Nml/(h $g_{cat}$))] for 1 h. Then a magnetization isotherm was collected again, and so forth. A total of four magnetization isotherms were collected for each catalyst after it was subjected to reforming conditions for 5 min and 1, 2, and 14 h. Each measurement took approximately 1 h, including all of the above-described steps.

### 2.4. $CO_2$ temperature-programmed desorption

$CO_2$ TPD measurements were carried out in a quartz reactor loaded with 50 mg of catalyst calcined in situ at 650 °C, reduced under pure hydrogen flow at the same temperature, then cooled to room temperature and contacted with pure carbon dioxide flow for 60 min, and finally flushed with argon flow for 30 min. The TPD ramp under Ar flow was started (20 °C/min) from room temperature to 650 °C, with the evolving gases continuously monitored by online mass spectrometry. No other gases besides $CO_2$ were detected at the reactor outlet. By integrating the TPD curves, the amount of reversibly adsorbed $CO_2$ was deduced and normalized to the highest amount corresponding to the Ni/CaO sample.

### 2.5. Calculations

Propane and carbon dioxide conversions were calculated on basis of feed and effluent concentrations, using $N_2$ as an internal standard. Except for the first analyses in the test, the carbon mass balance was always 100 ± 1%. The carbon monoxide and methane selectivities were calculated on the basis of effluent concentrations.

The turnover frequency (TOF) of a catalyst is defined as the number of reactant molecules converted to products over one active catalyst site per second. In the present case, each Ni atom on the outer surface of the Ni particles is considered an active site. The TOF of the Ni/support catalysts was calculated as follows. The number of exposed Ni surface sites ($N_{A,Ni}$) for each catalyst was calculated from the Ni loading

as well as the average Ni particle size determined from magnetic measurements ($D$). It was assumed that the Ni particles are spherical and that all outer surfaces are exposed to the reacting gases, which was demonstrated elsewhere as being a sound model [21]:

$$m_{\mathrm{Ni}} = m_{\mathrm{cat}} \cdot (\mathrm{wt\%\ Ni})/100, \tag{2}$$

$$V_{\mathrm{tot,Ni}} = m_{\mathrm{Ni}}/\rho_{\mathrm{Ni}}, \tag{3}$$

$$V_{\mathrm{part,Ni}} = 4/3 \cdot \pi \cdot (D/2)^3, \tag{4}$$

$$S_{\mathrm{Ni}} = (V_{\mathrm{tot,Ni}}/V_{\mathrm{part,Ni}}) \cdot 4 \cdot \pi \cdot (D/2)^2, \tag{5}$$

$$N_{\mathrm{A,Ni}} = S_{\mathrm{Ni}}/S_{\mathrm{spec,Ni}}, \tag{6}$$

and

$$N_{\mathrm{A,Ni,red}} = N_{\mathrm{A,Ni}} \cdot \mathrm{Reduction\%}/100, \tag{7}$$

where $D$ is the average Ni particle diameter calculated from magnetic measurements, $\rho_{\mathrm{Ni}}$ is the bulk density of Ni metal, $V_{\mathrm{part,Ni}}$ is the volume of each Ni particle, $V_{\mathrm{tot,Ni}}$ is the total volume of all Ni particles, $S_{\mathrm{Ni}}$ is the exposed Ni surface of all Ni particles, $S_{\mathrm{spec,Ni}}$ is the surface area of a Ni atom, and Reduction% is the degree of Ni reduction calculated from magnetic measurements.

The TOF of each catalyst after a given time on stream (TOS) was calculated using the following formula:

$$\mathrm{TOF}\ (\mathrm{s}^{-1}) = (C_{\mathrm{C_3H_8}}/100\%) \cdot \mathrm{Flow}_{\mathrm{C_3H_8}} \cdot A/N_{\mathrm{A,Ni,red}}, \tag{8}$$

where $C_{\mathrm{C_3H_8}}$ is the propane conversion (in %), $\mathrm{Flow}_{\mathrm{C_3H_8}}$ is the propane flow over the catalyst (mol/s), and $A$ is Avogadro's number.

## 3. Results

### 3.1. Catalytic testing

Results from the activity tests of all Ni/support catalysts for propane dry reforming at 600 °C are reported in Figs. 1 and 2. Equilibrium conversions and coke (C) selectivity under the applied test conditions were $C_{\mathrm{C_3H_8}} = 100\%$, $C_{\mathrm{CO_2}} = 57\%$, and $S_{\mathrm{C}} = 45\%$ [10]. Blank tests using the same feed and either an empty or an Mg(Al)O-filled reactor yielded zero and <0.3% propane conversion, respectively, at 600 °C [10].

Fig. 1 shows significant differences in both initial conversion and stability with time on stream (TOS) among the tested catalysts. The reproducibility of synthesis is good for the impregnated catalysts ($Ni/SiO_2$ and $Ni/Al_2O_3$; Fig. 1); however, for the catalysts prepared by coprecipitation, significant variation (i.e., by a factor of two) in activity and stability was observed between different catalyst batches, as shown in Fig. 1 [Ni/Mg(Al)O II and Ni/MgO]. Therefore, a systematic study of the activity-Ni particle size relationship requires performing independent measurements leading to TOF values on the same batch of catalyst, as in the present investigation. Reproducibility tests using the same batch of a Ni/Mg(Al)O variant (heat-treated somewhat differently from types I and II) in different tests gave very similar results (not reported). Thus, the reproducibility of the test procedure, as well as the homogeneity within one batch of catalyst, are considered satisfactory. Fig. 1 further shows that $Ni/SiO_2$ and $Ni/Al_2O_3$ had a strong initial deactivation before their performance stabilized.

The activity and stability of the Ni/Mg(Al)O II system varied significantly between different batches [Ni/Mg(Al)O II-a, b, and c]. The most active catalyst, Ni/Mg(Al)O II-c, showed initial deactivation, then reached a plateau of stable conversion, and finally deactivated completely after ~4000 min TOS. The Ni/Mg(Al)O II-a batch with medium activity showed initial deactivation followed by stable activity, whereas the least active batch (batch b) was stable throughout the test. The activity of the Ni/Mg(Al)O I catalyst (activated by Zr reduction) was similar to that of the corresponding material activated by $H_2$ reduction, with medium activity [Ni/Mg(Al)O II a]. This sample displayed remarkable stability with TOS over the 8000-min test period.

The results obtained for the Ni/MgO catalysts are similar to those observed for the Ni/Mg(Al)O catalysts. The least active catalyst (Ni/MgO-a) was rather stable during the test. The most active catalyst (Ni/MgO-b) had a period of initial deactivation, followed by a period of stable activity, before the activity dropped to zero after ~3500 min TOS. Visual inspection of Ni/MgO-b after the test showed that the catalyst changed in color from dark gray to white, indicating Ni oxidation. The Ni/CaO catalyst deactivated slowly throughout the test.

The relationship between product selectivity and propane conversion for the different Ni-based systems is reported in Fig. 2. Note that each plot represents the product selectivity observed during the life duration tests reported in Fig. 1. CO and $CH_4$ were observed to be main C-containing products for all of the tested catalysts. At very high propane conversions (i.e., at the start of each test), the carbon mass balances were poor, indicating appreciable coking rates. Small amounts of ethene were formed over the catalysts, although the selectivity was always <1%. The theoretical product selectivity ($S_{\mathrm{CO}}$, $S_{\mathrm{CH_4}}$) versus propane conversion at equilibrium is shown as dotted lines in Fig. 2. Thermodynamic data were taken from [22]. Only gaseous products were taken into account in these calculations. For $Ni/SiO_2$ and $Ni/Al_2O_3$, the methane selectivity approached equilibrium throughout the tests (8–100% propane conversion). For all Ni/Mg(Al)O and Ni/MgO samples, the methane selectivity was below equilibrium at all conversions and below 5% at 0–50% conversion. Ni/CaO also gave methane selectivities below equilibrium. However, the Ni/CaO test covered propane conversions only from 2 to 18%, for which even $Ni/SiO_2$ and $Ni/Al_2O_3$ gave low methane selectivity.

The results of a comparative test of methane dry reforming over Ni/Mg(Al)O II-a are presented in Fig. 3. The catalyst used in this experiment originated from the same synthesis batch as the propane dry reforming test performed over Ni/Mg(Al)O II-a, plotted in Fig. 1. A comparison of the two tests shows that methane dry reforming had a higher conversion than propane dry reforming, even though methane dry reforming was thermodynamically limited under the conditions used (i.e., 70% methane conversion and 43% $CO_2$ conversion at equilibrium), whereas propane conversion was thermodynamically complete.

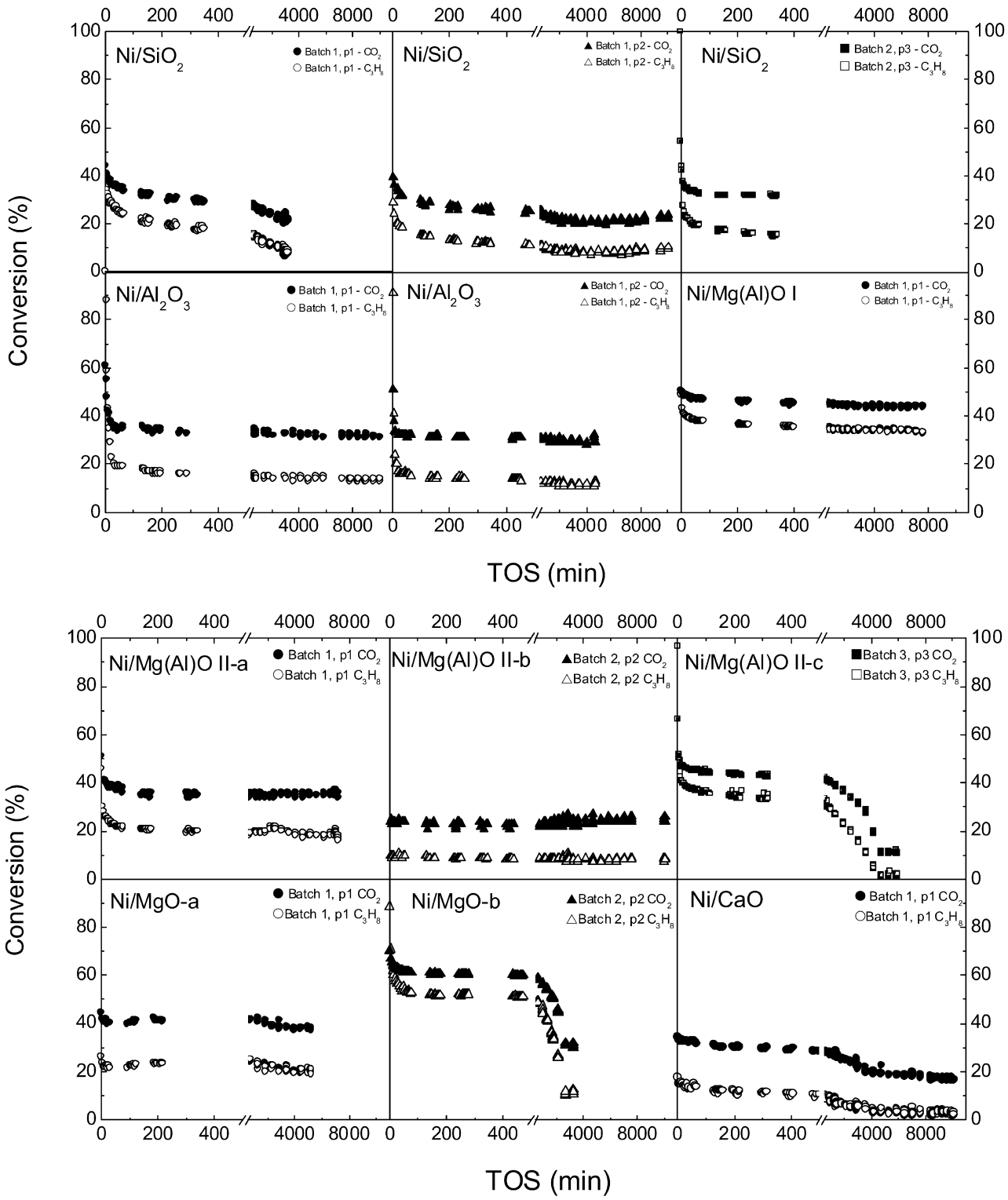


Fig. 1. Dry reforming of propane activity tests of Ni/support catalysts at 600 °C. Feed composition: $C_3H_8$:$CO_2$:$H_2$:$N_2$ (%) = 10:30:10:50.

### 3.2. Magnetic measurements

Nickel particle size and degree of nickel reduction for each catalyst before and during testing are reported in Table 2. For the $Ni/SiO_2$ system, the average Ni particle size was observed to vary between 8.0 and 8.5 nm, whereas the degree of Ni reduction was observed to decrease from 97% to 59% during the test period of 14 h. In addition, about 25–30% of the reduced Ni was found to be located in Ni particles larger than $D_c = 15$ nm. Interestingly, the remanent magnetization was found to decrease slightly with increasing TOS, indicating that a smaller fraction of the reduced Ni particles were larger than $D_c$ after being

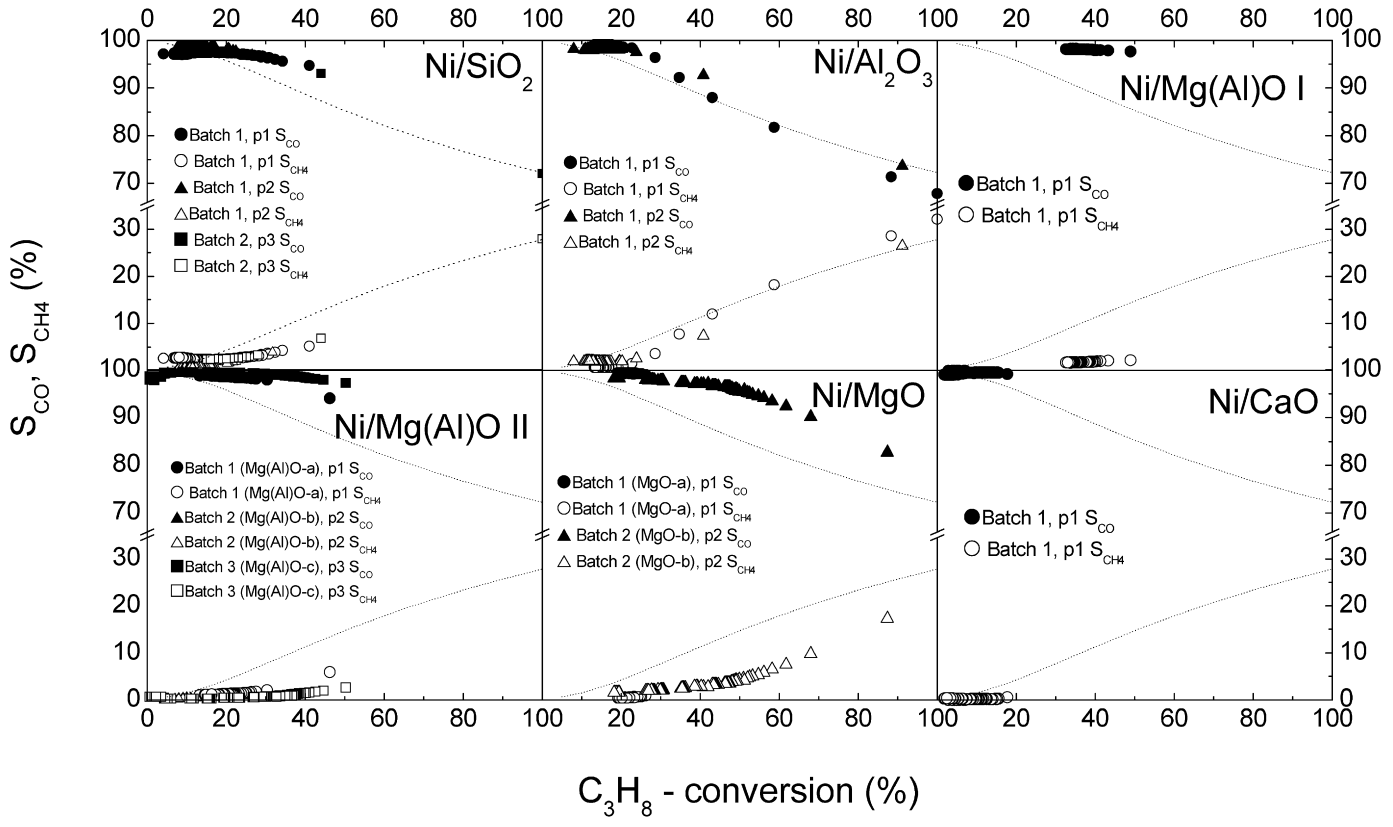


Fig. 2. Product selectivity versus propane conversion obtained over Ni/support catalysts at 600 °C. Calculated theoretical equilibrium selectivities at each conversion are shown as dotted lines.

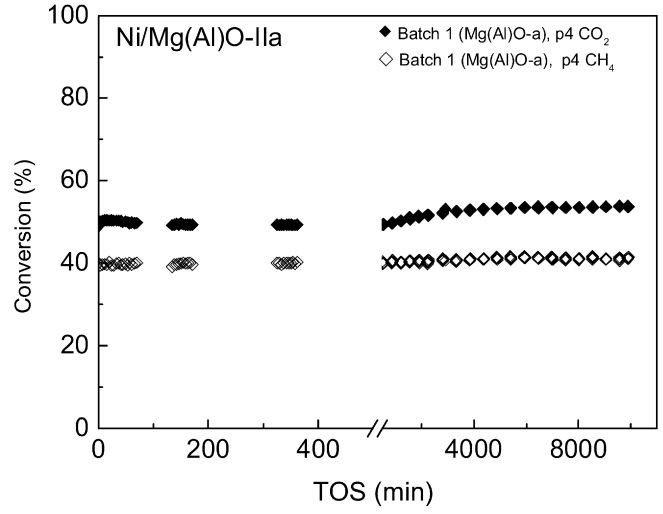


Fig. 3. Dry reforming of methane over Ni/Mg(Al)O II-a at 600 °C. Feed composition: $CH_4$:$CO_2$:$H_2$:$N_2$ (%) = 10:30:10:50.

exposed to reforming conditions. Another possible interpretation is that for very large particles, Weiss domains may have formed (equivalent to a collection of smaller particles) and the remanent magnetization may have decreased accordingly. According to Kroll et al. [23], the observation of Ni particles larger than $D_c$ for $Ni/SiO_2$ might depend on the pretreatment procedure. To correctly assess the morphological changes suggested by the magnetic measurements, we cross-checked our findings by TEM. Histograms of particle sizes indicated an average Ni particle diameter of 10.2 nm when only particles <15 nm were taken into account and of 13.9 nm when all particles were taken into account. It should be noted that when creating histograms from TEM measurements, all diameters were rounded up, leading to an overestimation of particle size. Therefore, the TEM results support the findings from the magnetic measurements.

The degree of Ni reduction in freshly reduced $Ni/Al_2O_3$ was only 60%, most likely due to the formation of $NiAl_2O_4$ spinel during the calcination step. According to the literature, spinel formation most likely occurs at elevated temperatures (see, e.g. [24]). The average Ni particle size and degree of Ni reduction of $Ni/Al_2O_3$ decreased from 7.5 to 6 nm and from 60 to 37% during the first 2 h on stream. Due to plugging of the reactor by coke, no magnetic measurements were made after 14 h on stream.

For the Ni/Mg(Al)O I system, a slight decrease in the degree of Ni reduction (from 59 to 46%) was observed with TOS. At the same time, the average Ni particle size slightly decreased from 7 to 5.5 nm. No remanence was observed.

The Ni/Mg(Al)O II-c system showed a very low degree of Ni reduction (from 22 to 17%). The average Ni particle was 4 to 5.5 nm throughout the tests. It should be noted that the test duration of magnetic measurements was shorter than the lifetime observed for this catalyst batch in the ordinary test reactor, as presented in Fig. 1.

For Ni/MgO-b, the degree of Ni reduction was also very low throughout the experiment (from 22 to 20%). The average Ni particle size decreased slightly or remained constant between

Table 2
Nickel phase characteristics extracted from magnetic measurements

| | Degree of reduction (%) | $D_2$ (Å) | $D_1$ (Å) | $D$ (nm) | $2M_r/M_s$ |
|---|---|---|---|---|---|
| | | Ni/$SiO_2$ | | | |
| Passivated | 87 | 57 | 114 | 8.5 | 0.294 |
| $H_2/N_2$ (10/90) | 97 | 47 | 111 | 8 | 0.285 |
| $C_3H_8/CO_2/H_2/N_2$ | 10/30/10/50 | | | | |
| TOS = 5 min | 86 | 58 | 113 | 8.5 | 0.291 |
| TOS = 1 h | 82 | 52 | 108 | 8 | 0.249 |
| TOS = 2 h | 96 | 56 | 109 | 8 | 0.253 |
| TOS ≈ 14 h | 59 | 59 | 109 | 8.5 | 0.255 |
| | | Ni/$Al_2O_3$ | | | |
| Passivated | 53 | 58 | 99 | 8 | 0.012 |
| $H_2/N_2$ (10/90) | 60 | 57 | 97 | 7.5 | 0.008 |
| $C_3H_8/CO_2/H_2/N_2$ | 10/30/10/50 | | | | |
| TOS = 1 h | 34 | 47 | 80 | 6.5 | 0.024 |
| TOS = 2 h | 37 | 44 | 79 | 6 | 0.022 |
| | | Ni/Mg(Al)O I | | | |
| Passivated | 51 | 42 | 89 | 6.5 | 0 |
| $H_2/N_2$ (10/90) | 59 | 51 | 89 | 7 | 0 |
| $C_3H_8/CO_2/H_2/N_2$ | 10/30/10/50 | | | | |
| TOS = 6.5 min | 58 | 41 | 79 | 6 | 0 |
| TOS = 1 h | 50 | 50 | 68 | 6 | 0 |
| TOS = 2 h | 50 | 44 | 69 | 5.5 | 0 |
| TOS ≈ 14 h | 46 | 49 | 66 | 5.5 | 0 |
| | | Ni/Mg(Al)O II-c | | | |
| Passivated | 11 | 38 | 69 | 5.5 | 0 |
| $H_2/N_2$ (10/90) | 22 | 34 | n.c. | n.c. | 0 |
| $C_3H_8/CO_2/H_2/N_2$ | 10/30/10/50 | | | | |
| TOS = 2 min | 17 | 33 | 49 | 4 | 0.014 |
| TOS = 1 h | 13 | 41 | 48 | 4.5 | 0 |
| TOS = 2 h | 15 | 44 | n.c. | n.c. | n.c. |
| TOS ≈ 14 h | 17 | 45 | n.c. | n.c. | n.c. |
| | | Ni/MgO-b | | | |
| Passivated | 15 | 49 | 68 | 6 | 0 |
| $H_2/N_2$ (10/90) | 22 | 38 | 55 | 4.5 | 0.034 |
| $C_3H_8/CO_2/H_2/N_2$ | 10/30/10/50 | | | | |
| TOS = 5 min | 21 | 39 | 67 | 5 | 0.023 |
| TOS = 1 h | 24 | 48 | 50 | 5 | 0.032 |
| TOS = 2 h | 20 | 45 | 47 | 4.5 | 0.005 |
| | | Ni/CaO | | | |
| Passivated | 72 | 62 | 114 | 8 | 0.0035 |
| $H_2/N_2$ (10/90) | 84 | 62 | 114 | 8 | 0.010 |
| $C_3H_8/CO_2/H_2/N_2$ | 10/30/10/50 | | | | |
| TOS = 5 min | 79 | 74 | 129 | 10 | n.c. |
| TOS = 1 h | 82 | 84 | 132 | 11 | 0.117 |
| TOS = 2 h | 84 | 76 | 133 | 10.5 | 0.134 |
| TOS ≈ 14 h | 89 | 95 | 138 | 11.5 | n.c. |

n.c. = not calculated.

4.5 and 5 nm during the first 2 h on stream. At TOS = 14 h, no propane conversion was observed, similar behavior to that observed for Ni/MgO-b during the lifetime study (Fig. 1).

The degree of Ni reduction on Ni/CaO was observed to increase slightly with TOS, with a maximum reduction of 89% at TOS = 14 h. The average Ni particle size increased from 8 to 11.5 nm, and the remanence increased from 1 to >13% during the test period.

### 3.3. $CO_2$ TPD measurements

$CO_2$ TPD curves obtained over each catalyst are plotted in Fig. 4. Most of the $CO_2$ TPD curves exhibited a single desorption peak with a maximum temperature within a 50–150 °C interval and spanning from 60 °C to about 500 °C, except for Ni/CaO with a TPD curve shifted to higher temperature, with a $T_{max}$ at 550 °C. Because Fig. 4 presents the $CO_2$ desorption versus temperature curves, the continued $CO_2$ desorption from Ni/CaO at 650 °C is not shown in the graph. It can be observed from the graph that the number and strength of basic sites increase from Ni/$SiO_2$ via Ni/$Al_2O_3$, Ni/Mg(Al)O, and Ni/MgO, to Ni/CaO. It also can be seen that the two close hydrotalcite materials, Ni/Mg(Al)O I and II-c, have different basic site concentrations, in line with the difference in BET surface areas (Table 1). The normalized concentration of basic sites of supported Ni catalysts derived from the TPD curves integration is reported in Table 3.

### 3.4. TOF

TOF was calculated on the basis on the aforementioned Ni dispersion for each catalyst during testing, as presented in Table 3. Note that due to the very rapid initial deactivation of most catalysts, the first data points (obtained after ca. 2–6 min on stream) should be considered with care. That considered, the data in Table 3 show that after the initial deactivation (<2 h on stream), the TOF for each catalyst is nearly constant with increasing TOS.

Plotting the TOF values calculated for the various catalysts after 1 h on stream as a function of the Ni particle diameter (i.e., Ni dispersion) leads to a straightforward relationship, as shown in Fig. 5. A decrease in Ni particle diameter in the range of 11–4.5 nm leads to a dramatic increase in TOF for the supported Ni catalysts, irrespective of the nature of the support. Although Fig. 5 presents the situation after only 1 h on stream, the trend is generally valid throughout the tests.

Comparing the mean stabilized TOFs calculated for the various catalysts as a function of the basicity ranking [$SiO_2$ < $Al_2O_3$ < Mg(Al)O I and II < MgO < CaO] shows no monotonous relationship between intrinsic activity and basicity (Table 3). Instead, a volcano-type relationship is seen, with a clear maximum of the intrinsic activity for the intermediate system Ni/Mg(Al)O II-c (Fig. 6A).

## 4. Discussion

### 4.1. Validity of TOF calculations

The conclusions of this study rely strongly on the calculated TOFs, which directly reflect the intrinsic activity of active sites. Thus, a discussion of the validity of TOF calculations is warranted. We made two assumptions during the calculations:

1. We assumed first that only reduced $Ni^0$ is active for propane dry reforming, whereas nickel oxide (NiO) and nickel carbide ($Ni_xC$), which are not detected by magnetic measure-

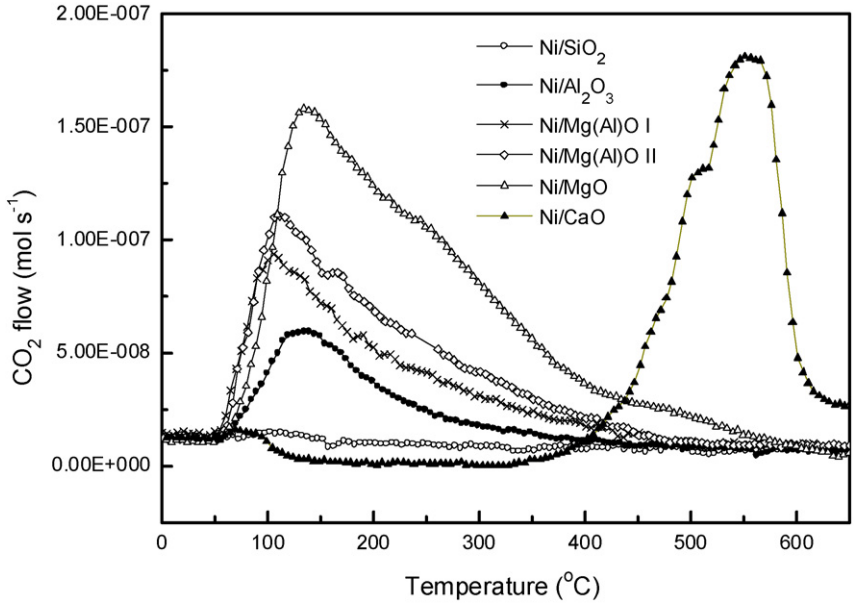


Fig. 4. $CO_2$ temperature-programmed desorption curves for the catalysts used in this study.

Table 3
Basicity from $CO_2$ TPD measurements. Turnover frequencies (TOF) versus time-on-stream (TOS)

| Catalyst | Concentration of basic sites, based on $CO_2$ TPD data[a] | TOS (min) | $D$ (nm) | $C_3H_8$ conversion (%) | TOF $\times 10^3$ ($s^{-1}$) |
|---|---|---|---|---|---|
| Ni/$SiO_2$ | 0.02 | 5 | 8.5 | 27 | 37 |
| | | 60 | 8 | 19 | 25 |
| | | 120 | 8 | 17 | 19 |
| | | ≈840 | 8.5 | 11 | 22 |
| Ni/$Al_2O_3$ | 0.24 | 60 | 6.5 | 16 | 44 |
| | | 120 | 6 | 15 | 36 |
| Ni/Mg(Al)O I | 0.39 | 6.5 | 6 | 43 | 71 |
| | | 60 | 6 | 38 | 73 |
| | | 120 | 5.5 | 36 | 63 |
| | | ≈840 | 5.5 | 34 | 65 |
| Ni/Mg(Al)O II-c | 0.54 | 2 | 4 | 50 | 172 |
| | | 60 | 4.5 | 37 | 188 |
| Ni/MgO-b | 0.84 | 5 | 5 | 68 | 233 |
| | | 60 | 5 | 48 | 145 |
| | | 120 | 4.5 | 47 | 153 |
| Ni/CaO | 1.0 | 5 | 10 | 15 | 18 |
| | | 60 | 11 | 14 | 18 |
| | | 120 | 10.5 | 12 | 14 |
| | | ≈840 | 11.5 | 10 | 12 |

[a] The concentration of basic sites has been normalized to Ni/CaO.

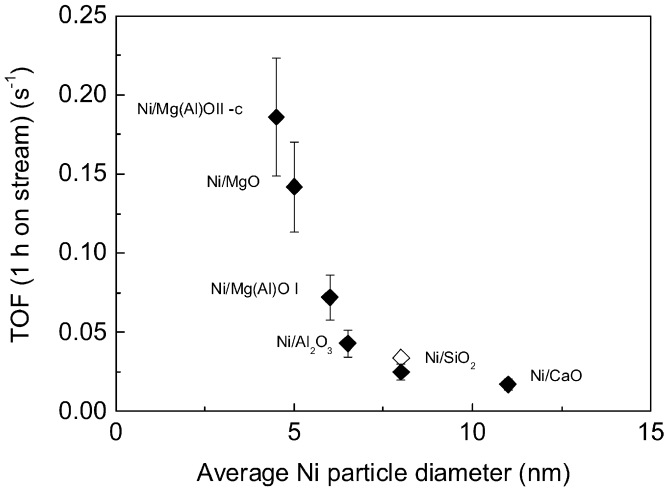


Fig. 5. TOF versus $D$ after 1 h on-stream for all tested catalysts. The black markers were calculated using particle diameters from magnetic measurements (cf. Tables 1 and 2). The white marker was calculated by using the particle diameter estimated from TEM analysis for Ni/$SiO_2$.

ments because they are nonferromagnetic, are not included in the calculations. The assumption that NiO is catalytically inactive is supported by several studies showing that the methane-reforming activity of an unreduced Ni catalyst is far inferior to that of a reduced Ni catalyst (see, e.g., [25]). For nickel carbide, the TOF calculations infer that the surface and bulk of each Ni particle are in the same zero-reduction state. Some previous reports contradicted this assumption, hypothesizing that whisker carbon formation proceeded by C diffusion through Ni particles, forming a carbide-like phase while the particle surface was still active [26]. However, recent studies [27,28], using HTEM and EXAFS in combination with catalytic activity measurements, have concluded that whisker formation proceeds at the outer surface of the active metal particle, and that carbide formation inside the particles starts at the onset of catalyst deactivation. Our results (i.e., stable TOF with TOS for coking catalysts) tend to agree with the feature of surface-diffusing carbon with no major bulk-process carbidization of Ni into nickel carbide. However, the effective transfer of carbon atoms from the hydrocarbon dissociation active centers (metallic nickel) to the particle extrusion faces into whiskers might involve interstitial forms of car-

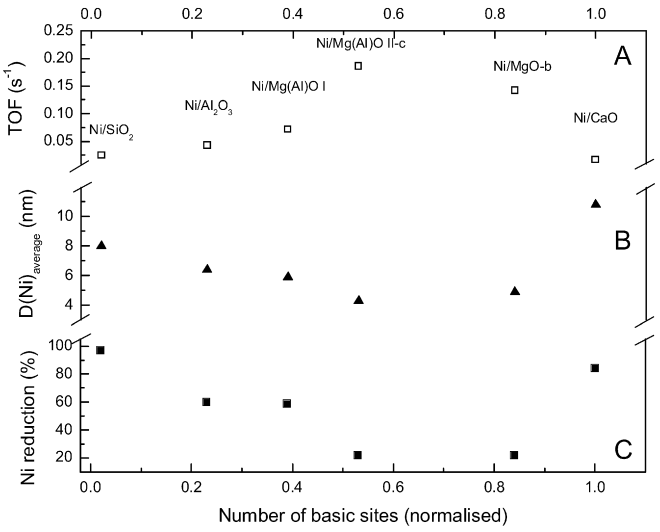


Fig. 6. (A) TOF after 1 h on-stream for all tested catalysts, (B) average Ni diameter and (C) degree of Ni reduction; all versus normalized concentration of basic sites from $CO_2$ TPD measurements. The values of Ni particle size and Ni reduction are those reported for reduced catalysts, see Table 2 (except for Ni/Mg(Al)O II, where Ni diameter after 2 min TOS is reported).

bon (leading to still-ferromagnetic Ni) throughout several surface layers of the Ni particles.

2. A second factor related to TOF calculations is the specific contribution of Ni particles larger than the critical diameter ($D_c = 15$ nm) detected for the case of the two extreme systems $Ni/SiO_2$ and Ni/CaO (Table 2). At $D > D_c$, the particle size cannot be determined from magnetic measurements. To investigate the effect of including larger particles, we determined TOF values for $Ni/SiO_2$ from both magnetic measurements and a full size distribution derived from TEM analysis. These two values are reported in Fig. 5 for comparison (with the open symbol representing data obtained by TEM). As can be seen, the TOF for $Ni/SiO_2$ increased slightly (from $25 \times 10^{-3}$ to $34 \times 10^{-3}$ $s^{-1}$) when the entire particle size distribution was included. However, including the larger particles found by TEM analysis does not alter the general relationship between Ni dispersion and intrinsic activity shown in Fig. 5, irrespective of the nature of the support.

### 4.2. Support influence

As a general comment, the $CO_2$ TPD results reported in Table 3 and Fig. 4 suggest a correlation between the normalized concentration of basic sites (able to reversibly adsorb $CO_2$) and basic strength. Note, however, the much stronger basicity for the CaO support, in agreement with theoretical calculations reported previously [29]. The formed carbonate species' high stability and large amount despite the low surface area strongly suggest that in this case, bulk carbonatization was achieved under the prevailing TPD conditions.

#### 4.2.1. Ni particle size

From the data reported in Table 2, together with the basicity measurements given in Table 3, an inverse volcano-type relationship between Ni particle size and surface basicity can be established, as depicted in Fig. 6B. The smallest Ni particle sizes are obtained for the medium basic Mg(Al)O-II. In turn, larger Ni particle diameters are observed for both the amphoteric $Ni/Al_2O_3$ and acidic $Ni/SiO_2$ and the more basic supports, Ni/MgO and Ni/CaO.

The BET surface areas of the catalysts decrease in the order Ni/Mg(Al)O II-c > Ni/Mg(Al)O I > Ni/MgO-b > $Ni/Al_2O_3 \sim Ni/SiO_2 \gg$ Ni/CaO. A similar order is found for the Ni particle size, except for the MgO support, which gives an intermediate Ni particle size between Ni/Mg(Al)O I and Ni/Mg(Al)O II-c despite having a lower specific surface area.

In terms of the degree of reduction of Ni particles, a strong linear coupling between nickel dispersion and degree of reduction is also seen by comparing Figs. 6B and 6C. This trend is characteristic of a strong Ni particle–support interaction, which keeps the smallest particles in a partially oxidized state, as in the case of the hydrotalcite-based supports.

Considering the reverse volcano-like relationship observed between Ni dispersion/reduction and surface basicity (Figs. 6B and 6C), several reports have suggested a possible inverse correlation between the number of basic or defect support sites and Ni particle diameter [30,31]. In the present study, such a trend of decreased Ni particle diameter with increasing number of basic sites also might be considered when disregarding Ni/CaO. As a matter of fact, the number of basic sites calculated for Ni/CaO should be interpreted with care. CaO is a very basic oxide. Due to its strong basic properties and its very low surface area, $CO_2$ may interact strongly with sites other than defects, favoring the formation of bulk carbonates and possibly leading to an overestimation of surface defects.

Previous studies [7–9] found that Ni particles supported on a highly basic support like lanthanum oxide ($La_2O_3$), which is almost completely carbonated under dry reforming conditions, are coated with a thin layer of lanthanum carbonate, which prevents sintering of particles and extraction of particles from the surface by carbon filaments during the reaction. In that case, surface area and defects are not concerned but only the faculty for carbonate phases to coat (several monolayers) and stabilize the metal particles.

To conclude, Ni particle distribution may be related to several parameters, most likely partly interconnected, which collectively can be considered a unique effect of metal–support interaction. These parameters include surface area, defect concentration, and basicity via carbonate coating. The dispersion and degree of reduction of nickel can be considered indicators of these various parameters.

#### 4.2.2. Catalyst activity

The results presented in Fig. 5 indicate unambiguously that a catalyst's TOF (i.e., nickel intrinsic activity) is strongly related to Ni particle size. Indeed, the graph displays an exponential shape, with a sharp increase in TOF at average Ni particle diameters below 7 nm. A similar trend was recently reported by Wei and Iglesia [12] for the dry reforming of methane over supported metal catalysts. Our data expand their findings while using a different method for determining exposed Ni area (mag-

netic measurements vs $H_2$ chemisorption) and a different reaction (propane vs methane). In addition, Wei and Iglesia used only one support for Ni catalysts (i.e., MgO), whereas our study covers a wide range of supports. Moreover, the relationship reported by these authors, as well as by Parmaliana et al. [30] in an earlier study of Ni particle size effect in methane steam reforming over Ni/MgO catalysts, was not as exponential as that observed in the present study.

Theoretical and experimental studies of model Ni surfaces have revealed that Ni defects have lower activation barriers toward methane activation than Ni terraces [32]. A recent study that used theoretical calculations to compare the activation barriers of C–C and C–H bond cleavage in ethene over Ni(111) and Ni(211) surfaces demonstrated that the activation barrier of C–C bond cleavage is far more structure-sensitive than that of C–H bond cleavage [33]. The results obtained in this study tend to indicate a stronger surface sensitivity of the propane dry reforming reaction compared with methane dry reforming, suggesting that either C–C bond cleavage or C oxidation is the rate-determining step for propane reforming, whereas only the C–H bond activation is of concern for methane dry reforming.

In this context, it is interesting to observe that the TOF versus $D$ relationship depicted in Fig. 5 is very similar to that reported by Carter et al. for ethane hydrogenolysis over 10 wt% $Ni/SiO_2$–$Al_2O_3$ with $D_{Ni} \approx 2$–10 nm at 267 °C [34]. This result could indicate that the rates of these two reactions are limited by the same reaction step, which would then not involve an oxygen-containing species. The origin of the structure sensitivity of both C–C and C–H bond activation should be related to the higher efficiency of defect Ni sites, which are numerous on small particles, compared with the denser and smoother planes dominant in larger particles. Steric factors favoring the C–C bond cleavage on out-of-plane Ni atoms might be the origin of such structure sensitivity; this effect would be much less prominent for the C–H bond cleavage in the smaller methane molecule.

#### 4.2.3. Catalyst stability

Three types of activity versus TOS behaviors were observed in this study:

1. $Ni/SiO_2$ and $Ni/Al_2O_3$. As can be seen in Tables 2 and 3, after a rapid initial deactivation, these two catalysts reached a stable TOF, but with a prominent decrease in the fraction of ferromagnetic Ni with TOS, accompanied by a slight decrease in the size of the ferromagnetic Ni particles for $Ni/Al_2O_3$. This result is consistent with a deactivation process related to coke formation, which has been reported to proceed more easily on larger Ni particles [35]. As such, this effect could derive from the buildup of an outer nonferromagnetic carbide-like thick layer with TOS, which would decrease the fraction of active metal. It is interesting to note that the TOF remained constant ($Ni/SiO_2$) or increased slightly ($Ni/Al_2O_3$) with TOS, again supporting the tight correlation between TOF and Ni particle size.
2. Ni/Mg(Al)O I and Ni/Mg(Al)O II-a and b. The two first catalysts reached rapidly steady conversion, Ni particle size distribution, and hence TOF after a rapid initial deactivation, whereas the less active Ni/Mg(Al)O II-b catalyst displayed stable activity throughout the test (Fig. 1; Tables 2 and 3). The steady-state level was different for each catalyst, increasing with a decrease in average Ni particle size. The rapid initial deactivation observed for these catalysts, as well as for the $Ni/SiO_2$ and $Ni/Al_2O_3$ catalysts, was in all cases accompanied by a poor carbon balance, indicating that the initial deactivation was essentially due to carbide and/or coke formation.
   Considering now the good steady-state performance of the catalysts that display moderate basicity, it has previously been shown that $CO_2$ species trapped as unstable surface carbonate on a Mg(Al)O support are able to oxidize the Ni surface during pulse experiments in a temporal analysis of products (TAP) reactor [10]. We thus can deduce that such an oxygen spillover arising from the continuous decomposition of surrounding surface carbonates improves the C/H/O balance on the Ni surface, favoring CO (versus carbon deposits) formation. However, overly efficient oxygen transfer from the support to the Ni surface could contribute to the sudden death of the most active Ni/MgO-b and Ni/Mg(Al)O II-c catalysts due to Ni oxidation after ∼60 h on stream.
3. Ni/CaO. As can be seen from Tables 1 and 2, Ni/CaO displayed a stable reduction state with TOS but with increasing Ni particle size and decreasing TOF throughout the test. This result clearly indicates that the Ni particles sintered with TOS, most likely due to the very poor surface area of that support, preventing any stabilization effect via particle–support interaction. Conversely, the blocking of Ni particles due to coke formation is limited, in line with the above statement because the particles that are not stabilized on the support can be hardly deactivated by encapsulating carbon. The decrease in TOF with an increasing particle size is in agreement with the trend reported in Fig. 5.

Finally, comparing the $CH_4$ and CO selectivities over the various catalysts during aging tests (Fig. 2), note that the $CH_4$ selectivity over $Ni/SiO_2$ and $Ni/Al_2O_3$ approached equilibrium throughout the tests, but was far inferior to the equilibrium amount over all catalysts with more basic carrier materials [Mg(Al)O, MgO, CaO]. This difference may be simply related to the surface acidity of the $Ni/SiO_2$ and $Ni/Al_2O_3$ supports. An early effect would be the favoring of direct cracking of propane molecules into methane over the support acid sites, after an initial deactivation of the Ni particles. Another effect would be the favoring of cracking of propane into methane on the metallic surface due to the more pronounced metallic state of the Ni particles on these catalysts and their poor metal dispersion, whereas the partially oxidized state of nickel over the more basic systems prevents cracking of propane into methane, in turn favoring its partial oxidation into carbon monoxide. The relative importance of these two effects is likely to depend on the Ni dispersion and on the effective acidity of the support.

## 5. Conclusion

In this work, propane dry reforming over Ni based catalysts was found to be highly structure-sensitive, as demonstrated by an exponential relationship between intrinsic activity (TOF) and mean particle size of metallic nickel particles. The structure sensitivity was more marked than that for methane dry reforming [12,30] due to the specificity of C–C bond cleavage compared with C–H bond cleavage. In parallel, the intermediate basicity observed on such systems as Ni/Mg(Al)O and Ni/MgO ensures the highest stability and catalytic performance of the active Ni phase, including low methane selectivity. This intermediate basicity might correspond to an optimum of $CO_2$/carbonate equilibrium, ensuring permanent feeding of the Ni surface with oxygen from carbonate decomposition and sufficiently stable carbonate to protect the Ni particles from deactivation by carbon buildup and metal sintering. Our findings indicate that the best-performing systems displayed the largest nickel dispersion combined with moderate support basicity. Monitoring this complex interconnection of various parameters, including surface area, defect concentration, and basicity, and their varying impacts on dry reforming of propane or methane, is a prerequisite for optimizing catalytic systems and process operating conditions for reforming real feedstocks of natural gas containing methane, higher hydrocarbons, and $CO_2$.

## Acknowledgment

This project was supported by the Norwegian Research Council under the KOSK program (contract 139193/431).

## References

[1] S.C. Tsang, J.B. Claridge, M.L.H. Green, Catal. Today 23 (1995) 3.
[2] Z.L. Zhang, X.E. Verykios, J. Chem. Soc. Chem. Commun. (1995) 71.
[3] O. Yamazaki, K. Tomishige, K. Fujimoto, Appl. Catal. A Gen. 136 (1996) 49.
[4] K. Tomishige, K. Fujimoto, Catal. Surv. Jpn. 2 (1998) 3.
[5] F. Besenbacher, I. Chorkendorff, B.S. Clausen, B. Hammer, A.M. Molenbroek, J.K. Nørskov, I. Stensgaard, Science 279 (1998) 1913.
[6] T. Shishido, M. Sukenobu, H. Morioka, R. Furukawa, H. Shirahase, K. Takehira, Catal. Lett. 73 (2001) 21.
[7] Z.L. Zhang, X.E. Verykios, Appl. Catal. 138 (1996) 109.
[8] Z.L. Zhang, X.E. Verykios, S.M. MacDonald, S. Affrosman, J. Phys. Chem. 100 (1996) 744.
[9] Å. Slagtern, Y. Schuurman, C. Leclercq, X. Verykios, C. Mirodatos, J. Catal. 172 (1997) 118.
[10] A. Olafsen, Å. Slagtern, I.M. Dahl, U. Olsbye, Y. Schuurman, C. Mirodatos, J. Catal. 229 (2005) 163.
[11] D.E. Ramaker, J. de Graaf, J.A.R. van Veen, D.C. Koningsberger, J. Catal. 203 (1) (2001) 7.
[12] J. Wei, E. Iglesia, J. Catal. 224 (2004) 370;
J. Wei, E. Iglesia, Angew. Chem. 43 (2004) 3685;
J. Wei, E. Iglesia, J. Phys. Chem. B 108 (2004) 7253.
[13] L. Pinaeva, Y. Schuurman, C. Mirodatos, in: M. Maroto-Valer, C. Song, Y. Soong (Eds.), Environmental Challenges and Greenhouse Gas Control for Fossil Fuel Utilization in the 21st Century, Kluwer Academic/Plenum Publishers, New York, 2002, p. 313.
[14] F. Solymosi, P. Tolmacsov, K. Kedves, J. Catal. 216 (1–2) (2003) 377.
[15] D. Sutton, J.F. Moisan, J.R.H. Ross, Catal. Lett. 75 (2001) 175.
[16] F. Solymosi, P. Tolmacsov, T.S. Zakar, J. Catal. 233 (2005) 51.
[17] A. Olafsen, C. Daniel, Y. Schuurman, L.B. Råberg, U. Olsbye, C. Mirodatos, Catal. Today 115 (1–4) (2006) 179.
[18] P.W. Selwood, Chemisorption and Magnetization, Academic Press, New York, 1975.
[19] J.-A. Dalmon, in: B. Imelik, J.C. Védrine (Eds.), Catalyst Characterizaton, in: Physical Techniques for Solid Materials, Plenum Press, New York, 1994.
[20] C. Mirodatos, H. Praliaud, M. Primet, J. Catal. 107 (1987) 275.
[21] K.O. Christensen, D. Chen, R. Lødeng, A. Holmen, Appl. Catal. A Gen. 314 (2006) 9.
[22] NIST Standard Reference Database 85, NIST/TRC Table Database, WinTable (2004).
[23] V.C.H. Kroll, H.M. Swaan, C. Mirodatos, J. Catal. 161 (1996) 409.
[24] G.R. Galavas, C. Phichitkul, G.E. Voecks, J. Catal. 88 (1984) 54.
[25] F. van Looij, J.W. Geus, J. Catal. 168 (1997) 154.
[26] R.T.K. Baker, M.A. Barber, P.S. Harris, F.S. Feates, R.J. Waite, J. Catal. 26 (1972) 51.
[27] S. Takenaka, H. Ogihara, K. Otsuka, J. Catal. 208 (1) (2002) 54.
[28] S. Helveg, C. López-Cartes, J. Sehested, P.L. Hansen, B.S. Clausen, J.R. Rostrup-Nielsen, F. Abild-Pedersen, J.K. Nørskov, Nature 427 (2004) 426.
[29] M.B. Jensen, L.G.M. Pettersson, O. Swang, U. Olsbye, J. Phys. Chem. B 109 (2005) 16774.
[30] A. Parmaliana, F. Arena, F. Frusteri, S. Coluccia, L. Marchese, G. Martra, A.L. Chuvilin, J. Catal. 141 (1) (1993) 34.
[31] Z. Gandao, B. Coq, L.C. de Menorval, D. Tichit, Appl. Catal. A Gen. 147 (1996) 395.
[32] F. Abild-Pedersen, O. Lytken, J. Engbæk, G. Nielsen, I. Chorkendorff, J.K. Nørskov, Surf. Sci. 590 (2005) 127.
[33] R.T. Vang, K. Honkala, S. Dahl, E.K. Vestergaard, J. Schnadt, E. Lægsgaard, B.J. Clausen, J.K. Nørskov, F. Besenbacher, Nat. Mater. 4 (2005) 160.
[34] J.L. Carter, J.A. Cusumano, J.H. Sinfelt, J. Phys. Chem. 70 (7) (1966) 2257.
[35] J.A. Lercher, J.H. Bitter, W. Hally, W. Niessen, K. Seshan, Stud. Surf. Sci. Catal. 101 (1996) 463.